ADVANCED SCIENCE
Open Access
www.advancedscience.com

Cu_2O Nanoparticles with Both {100} and {111} Facets for Enhancing the Selectivity and Activity of CO_2 Electroreduction to Ethylene

Yugang Gao, Qian Wu, Xizhuang Liang, Zeyan Wang, Zhaoke Zheng, Peng Wang, Yuanyuan Liu, Ying Dai, Myung-Hwan Whangbo, and Baibiao Huang**

Cu_2O nanoparticles (NPs) enclosed with different crystal facets, namely, c-Cu_2O NPs with {100} facets, o-Cu_2O NPs with {111} facets, and t-Cu_2O NPs with both {111} and {100} facets, are prepared and their electrocatalytic properties for the reduction of CO_2 to C_2H_4 are evaluated. It is shown that the selectivity and activity of the C_2H_4 production depend strongly on the crystal facets exposed in Cu_2O NPs. The selectivities for the C_2H_4 production increases in the order, c-Cu_2O < o-Cu_2O < t-Cu_2O, (with $FE_{C_2H_4}$ = 38%, 45%, and 59%, respectively). This study suggests that Cu_2O NPs are more likely responsible for the selectivity and activity for the C_2H_4 production than the metallic Cu NPs produced on the surface of Cu_2O NPs. This work provides a new route for enhancing the selectivity of the electrocatalytic CO_2 reduction by crystal facet engineering.

Carbon dioxide (CO_2) is highly responsible for the global warming and climate change, which makes it urgent to reduce the amount of CO_2 in atmosphere.[1,2] In reducing the amount of CO_2, the electrocatalytic CO_2 reduction reaction (CO_2RR) is attractive because it can transform CO_2 into high-valued feedstocks with high efficiency and can be combined easily with renewable energy sources such as solar or wind energy.[3–7] Since the CO_2RR leads to various carbon products, it is necessary to improve the selectivity and activity for a single desired product. The production of C1 species such as carbon monoxide or formic acid has reached a very high selectivity (over 90%),[8–14] but those of multi-carbon species with higher commercial values have not.[15]

Among the available electrocatalysts, copper is unique because it can produce various hydrocarbons and alcohols and because it can absorb CO intermediates well, facilitating the subsequent C–C coupling for C_{2+} production.[16–19] Ethylene (C_2H_4), an important raw material, is one of the main C2 products over Cu electrodes.[20] However, due to the simultaneous production of H_2 and other C1 species (i.e., CO, CH_4), the Faradaic efficiency for the production of C_2H_4 ($FE_{C_2H_4}$) on metallic Cu is usually low.[21–24] Efforts to improve the $FE_{C_2H_4}$ of Cu-based catalysts have focused on optimizing the sizes, morphologies, and exposed crystal facets of metallic Cu NPs.[25–31] In producing C_2H_4 with high selectivity, Cu_2O NPs have recently been found to be more effective than metallic Cu NPs. For example, the $FE_{C_2H_4}$ of 36% was achieved from a Cu/Cu_2O catalyst prepared by electro-redeposition method,[32] and that of 57% from a nanodendritic Cu catalyst.[33] Cu_2O NPs show a good performance probably because the low-coordinate Cu^+ ions present on the surface help the C–C coupling, thereby boosting the C_2H_4 production.[34–40]

In controlling the activity and selectivity of electrocatalysts, it is important to understand how they are affected by the crystal facets. The crystal facets of metallic Cu NPs have a strong influence on the selectivity and activity of their catalytic reactions. For example, the Cu {111} facets lead preferentially to CH_4, while the Cu {100} and some high index planes to C2 products.[33,41] Studies on Cu_2O NPs showed that those with different crystal facets exhibit different stabilities and different catalytic activities.[42–44] For example, for the propylene oxidation under high temperature, Cu_2O NPs enclosed with the {111} facets are more catalytically active than those enclosed with the {100} or {110} facets. During a photocatalytic degradation of methyl orange on Cu_2O, electron transfer occurs from the

Dr. Y. Gao, Dr. X. Liang, Prof. Z. Wang, Prof. Z. Zheng, Prof. P. Wang, Prof. Y. Liu, Prof. M.-H. Whangbo, Prof. B. Huang
State Key Laboratory of Crystal Materials
Shandong University
Jinan 250100, China
E-mail: wangzeyan@sdu.edu.cn; bbhuang@sdu.edu.cn

Dr. Q. Wu, Prof. Y. Dai
School of Physics
Shandong University
Jinan 250100, China

Prof. M.-H. Whangbo
Department of Chemistry
North Carolina State University
Raleigh, NC 27695-8204, USA

Prof. M.-H. Whangbo
State Key Laboratory of Structural Chemistry
Fujian Institute of Research on the Structure of Matter (FJIRSM)
Chinese Academy of Sciences (CAS)
Fuzhou 350002, China

The ORCID identification number(s) for the author(s) of this article can be found under https://doi.org/10.1002/advs.201902820.

DOI: 10.1002/advs.201902820

{100} and {110} to {111} facets.[45] During the electrochemical reduction over Cu_2O under negative potentials, metallic Cu NPs are formed on the surface of Cu_2O. It has not been unequivocal whether or not active catalysts during CO_2RR are the metallic Cu NPs produced on the surface of Cu_2O.[46–48] The Cu NPs produced from Cu_2O NPs with different morphologies differ in size and aggregation, affecting their selectivity and activity for the C_2H_4 production.[39] These observations prompt us to examine if the metallic Cu NPs derived from Cu_2O NPs possessing different crystal facets lead to different selectivities and different activities for the C_2H_4 production and consequently whether the Cu_2O or the metallic Cu NPs are responsible for the selectivity and activity of the CO_2RR.

We explored these questions by preparing Cu_2O NPs enclosed with different crystal facets, namely, cubic Cu_2O (c-Cu_2O) NPs with {100} facets, octahedral Cu_2O (o-Cu_2O) NPs with {111} facets, and truncated-octahedral Cu_2O (t-Cu_2O) NPs with both {111} and {100} facets, and then by evaluating the effect of the exposed crystal facets on the selectivity and activity for the C_2H_4 production. Our study shows that the selectivity and activity of the C_2H_4 production are strongly affected by the crystal facets exposed in Cu_2O NPs. We show that the selectivities of the Cu_2O NPs for the C_2H_4 production increases in the order, c-Cu_2O < o-Cu_2O < t-Cu_2O, (with $FE_{C_2H_4}$ = 38%, 45%, and 59%, respectively). Our study suggests strongly that Cu_2O NPs are more likely responsible for the selectivity and activity for the C_2H_4 production than are the metallic Cu NPs produced on the surface of Cu_2O NPs.

The Cu_2O NPs were prepared by a wet chemical reduction method.[49,50] A mixture of Cu_2O and carbon black was deposited on a glassy carbon electrode (GCE) to form a working electrode for the CO_2RR (for details, see the Supporting Information). The crystal structure of the samples are determined by X-ray diffraction (XRD) (Figure S1, Supporting Information). The morphologies of the as-prepared c-Cu_2O, o-Cu_2O, and t-Cu_2O NPs were characterized by scanning electron microscopy (SEM). The three kinds of Cu_2O NPs have the sizes of 600–1000 nm, but their morphologies are different. c-Cu_2O NPs exhibit cubic nanostructures (**Figure 1**a,b) enclosed with six {100} planes. The o-Cu_2O NPs exhibit an octahedral morphology (Figure 1c,d) exposed with eight Cu_2O {111} planes. The t-Cu_2O NPs exhibit a polyhedral morphology (Figure 1e,f) exposed with both {100} and {111} facets.[45,51]

We now compare the CO_2RR performances of the three Cu_2O electrodes by performing potentiostatic measurements in an H-type electrochemical cell with CO_2 saturated aqueous 0.5 M $KHCO_3$ as electrolyte. The amounts of the gaseous and liquid products were determined by gas chromatography (GC) and nuclear magnetic resonance (NMR), respectively (Figures S2 and S3, Supporting Information). To examine the selectivity for the C_2H_4 production, we determine the Faradaic efficiency, $FE_{C_2H_4} = Q_{C_2H_4}/Q_{tot}$, where $Q_{C_2H_4}$ is the amount of charge consumed to produce C_2H_4, and Q_{tot} the charge consumed to produce all products (for details see the Supporting Information). The $FE_{C_2H_4}$ values for the three Cu_2O electrodes are compared in **Figure 2**a. t-Cu_2O NPs exhibit the highest selectivity at five selected potentials ranging from −0.9 to −1.3 V relative to reversible hydrogen electrode (RHE) (see Figure S4 in the Supporting Information for RHE calibration). The

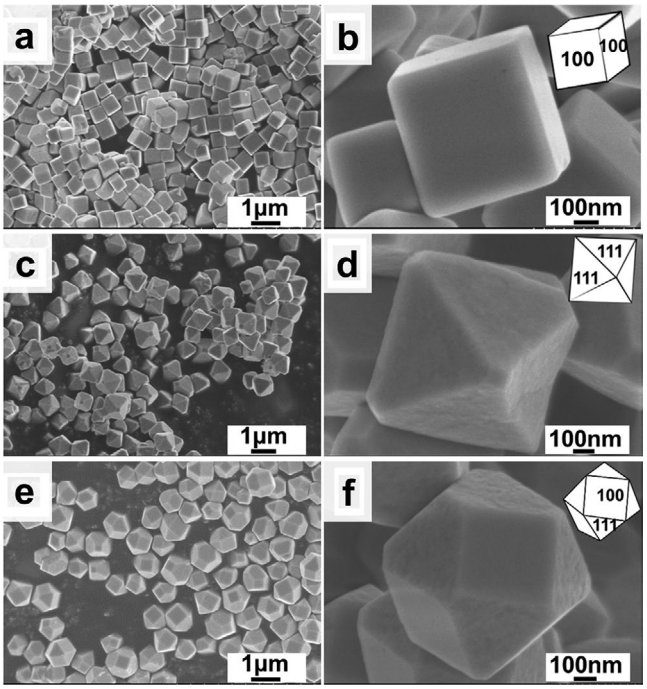

Figure 1. SEM images of a,b) c-Cu_2O NPs, c,d) o-Cu_2O NPs, and e,f) t-Cu_2O NPs.

maximum $FE_{C_2H_4}$ reaches 59% at −1.1 V, which is comparable to the highest achieved in $KHCO_3$ so far by using plasma-activated copper (60% at −1.1 V).[31] The maximum $FE_{C_2H_4}$ for other Cu_2O NPs are lower, namely, 45% at −1.1 V for o-Cu_2O NPs, and 40% at −1.2 V for c-Cu_2O NPs. We evaluate the activities of the three Cu_2O NPs for the C_2H_4 production by calculating the currents consumed for the production, $j_{C_2H_4} = FE_{C_2H_4} \times j_{total}$, where j_{total} is the total current used from the potentiostatic measurements. At any given potential, the $j_{C_2H_4}$ for t-Cu_2O NPs is higher than those for o-Cu_2O and c-Cu_2O NPs (Figure 2b). Furthermore, the $j_{C_2H_4}$ for t-Cu_2O and o-Cu_2O NPs increases steadily with increasing the potential, but this is not the case for c-Cu_2O NPs (Figure 2b). We now examine the stability of Cu_2O NPs by performing potentiostatic tests at a potential of −1.1 V for 2 h (Figure 2c). The current density of c-Cu_2O, o-Cu_2O, t-Cu_2O NPs is maintained at about 11, 17, and 22 mA cm^{-2}, respectively with only ≈5% decrease in 2 h (For more details of the stability test, see Figure S5, Supporting Information). To probe the kinetics of the C_2H_4 production, we examine the Tafel plots for the three Cu_2O NPs (Figure 2d). The Tafel slope for t-Cu_2O NPs (75 mV dec^{-1}) is lower than those of o-Cu_2O (82 mV dec^{-1}) and c-Cu_2O (97 mV dec^{-1}) NPs so that it has the lowest activation energy for the CO_2RR. In short, for the CO_2RR toward C_2H_4, t-Cu_2O NPs exposed with {100} and {111} facets exhibit a better selectivity, activity than do o-Cu_2O NPs with {111} facets and c-Cu_2O NPs exposed with {100} facets.

In our discussions so far, we have not examined the question whether the catalytic activities of the Cu_2O NPs are the intrinsic properties of these NPs or they originate from the metallic Cu NPs on the surface of the Cu_2O NPs produced during the CO_2RR. To explore this question, we carried out transmission electron microscopy (TEM) measurements for the Cu_2O NPs

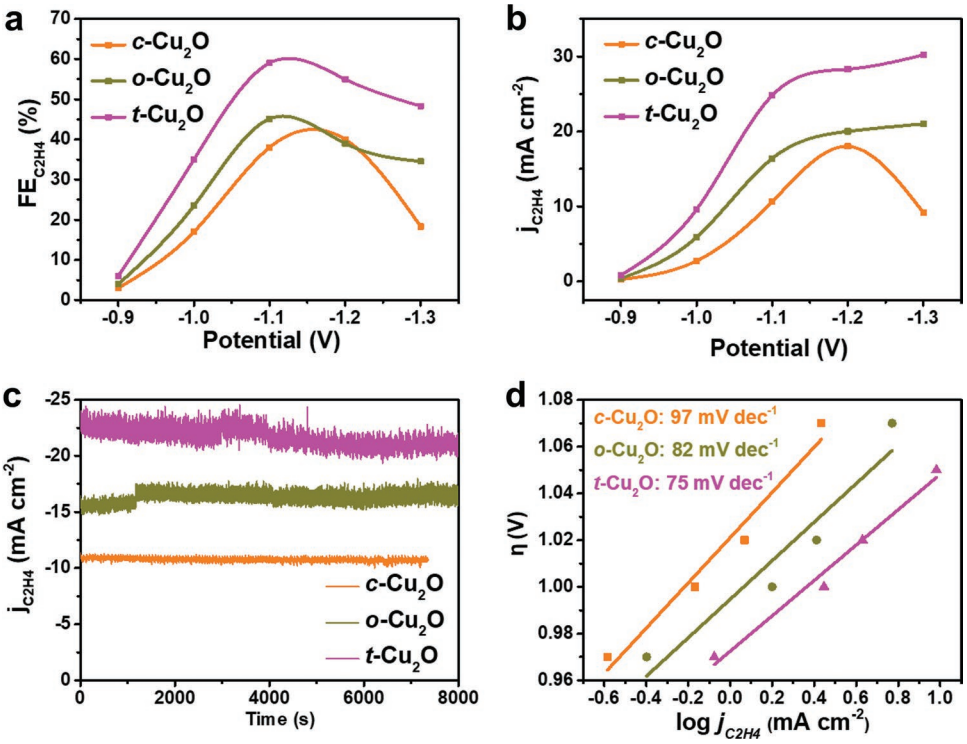

Figure 2. a) $FE_{C_2H_4}$ values for the c-Cu_2O, o-Cu_2O, and t-Cu_2O NPs as a function of the potential. b) $j_{C_2H_4}$ values for the c-Cu_2O, o-Cu_2O, and t-Cu_2O NPs as a function of the potential. c) $j_{C_2H_4}$ values for the c-Cu_2O, o-Cu_2O, and t-Cu_2O NPs at −1.1 V as a function of the reaction time. d) Tafel plots for the c-Cu_2O, o-Cu_2O, and t-Cu_2O NPs.

after the CO_2RR. As shown in **Figure 3**a–c, the morphologies of all the three Cu_2O nanoparticles can be well preserved after the stability test, with only some tiny nanoparticles on the surfaces, which could be probably ascribed to the Cu nanoparticles formed during electroreduction process. This finding is consistent with the stability tests discussed in Figure 2c.[52] To further probe the change on composition and valence state of Cu_2O NPs after electrocatalytic reaction, Cu LMM Auger spectra were performed on the three Cu_2O samples before and after their use in the CO_2RR (Figure 3d–f). The peaks of Cu_2O and Cu are observed at 570.6 and 567.5 eV, respectively. The Auger spectra confirmed that before the stability test, all the three Cu_2O samples are mainly consisted of Cu^+. While, a small part (≈5%) of Cu^0 can be observed beside Cu^+ after the stability test. According to these results, we conclude that the electrocatalytic activity of Cu_2O NPs is an intrinsic property of these oxides rather than the metallic Cu NPs produced on their surfaces.

To probe a possible reaction mechanism for the CO_2RR, we examine how the amount of the gaseous products, C_2H_4, CH_4, CO, and H_2, arising from c-Cu_2O, o-Cu_2O, and t-Cu_2O NPs, vary as a function of the potential as shown in Figure S6 (Supporting Information). The production of C_2H_4 and CO over all the three samples exhibit similar trends, where the $FE_{C_2H_4}$ initially increased sharply then decreased as the applied potential increased, while, the FE_{CO} decreased constantly with the increase of potential. This confirms that adsorbed CO species are intermediates for C_2H_4 production during CO_2RR. Comparing to the production of C_2H_4, the formation of CH_4 is much lower. That indicates C–C coupling to form C_2H_4 from adsorbed CO intermediates is preferable than does the formation of CH_4 on the surface of Cu_2O NPs. The production of hydrogen from the three Cu_2O NPs enclosed with different crystal facets are quite different. The FE_{H_2} for c-Cu_2O is high (≈50%) at −0.9 V versus RHE, which sharply decreased with the increase of applied potential, then increased as the potential is more negative than −1.1 V versus RHE. For o-Cu_2O, the FE_{H_2} is relatively lower than that from c-Cu_2O as the potential is below (≈30%) −1.1 V versus RHE, then increased quickly as the potential further increased. This indicates the production of H_2 from {100} facets of Cu_2O could be more preferable than over Cu_2O {111} facets, which can explain why the $FE_{C_2H_4}$ over o-Cu_2O is higher than that of c-Cu_2O. However, for t-Cu_2O, the FE_{H_2} was kept below 30% as the potential ranging from −0.9 to −1.3 V versus RHE. This indicates the production of H_2 can be effectively suppressed in t-Cu_2O enclosed by both {100} and {111} facets, which lead to the highest $FE_{C_2H_4}$ among the three samples.

To gain insight into the reason why t-Cu_2O has a better performance for the C_2H_4 production than does c-Cu_2O and o-Cu_2O NPs, we carry out DFT calculations to examine the adsorption capabilities of the reaction intermediate CO as well as the product C_2H_4 on the Cu_2O {100} facets, {111} facets and the joint interface between {100} and {111} facets.[53,54] As shown in **Figure 4**, CO is more strongly adsorbed on the Cu_2O {100} facets and the joint interface between {100} and {111} facets than on the Cu_2O {111} facets. This would subsequently facilitate the C–C coupling to produce C_{2+} products during

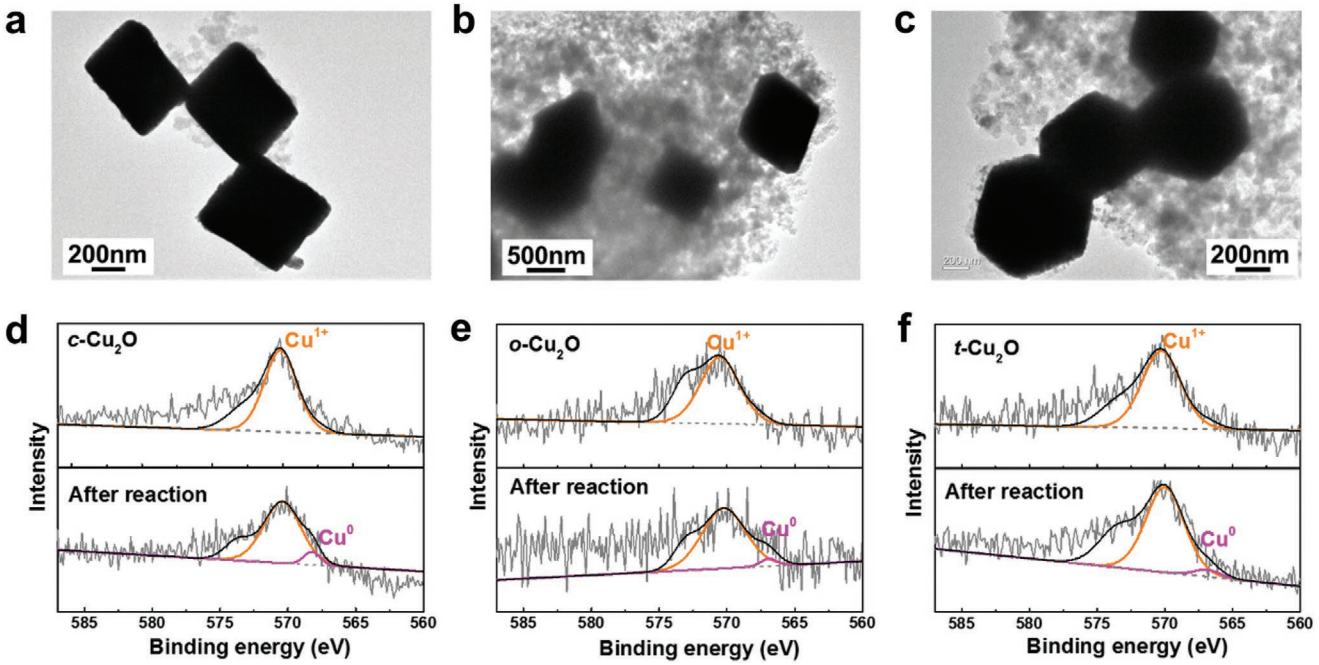

Figure 3. TEM images and Cu LMM Auger spectra of a,d) c-Cu_2O, b,e) o-Cu_2O, and c,f) t-Cu_2O after CO_2RR, respectively.

CO_2RR. On the other hand, C_2H_4 can be adsorbed more weakly on the joint interface between Cu_2O {100} and {111} facets and Cu_2O {111} facets than on the Cu_2O {100} facets. That means c-Cu_2O enclosed by {100} facets could facilitate the C–C coupling to produce C_{2+} products, but the formed C_{2+} products (e.g., C_2H_4) can hardly escape from the surface of Cu_2O {100} facet because of its stronger adsorption ability of C_2H_4. For o-Cu_2O enclosed by {111} facets, although the adsorption of CO intermediates is lower than that on Cu_2O {100} facets, once C_2H_4 was formed, it can be easily desorbed from the surface of Cu_2O {111} facets because of its weaker adsorption ability. Meanwhile, for t-Cu_2O enclosed by both {100} and {111} facets, the CO intermediates can not only be strongly adsorbed on the joint interface between {100} and {111} facets to promote the C–C coupling, but also the as-formed C_2H_4 can be easily desorbed from the joint interface to promote the C_2H_4 production.

In addition, the reason why t-Cu_2O provides a much better catalytic performance than does c-Cu_2O and o-Cu_2O may be related to the fact that the Fermi level of Cu_2O is lower on the {111} than on the {100} facets.[54] This could subsequently facilitate the charge transfer between Cu_2O {111} and {100} facets, and further promote the multielectron involved kinetics for ethylene production in Cu_2O nanoparticles enclosed by both {111} and {100} facets (**Figure 5**a–c).[55–57]

In summary, the t-Cu_2O NPs enclosed with both {100} and {111} facets exhibit the $FE_{C_2H_4}$ and $j_{C_2H_4}$ values of 59% and

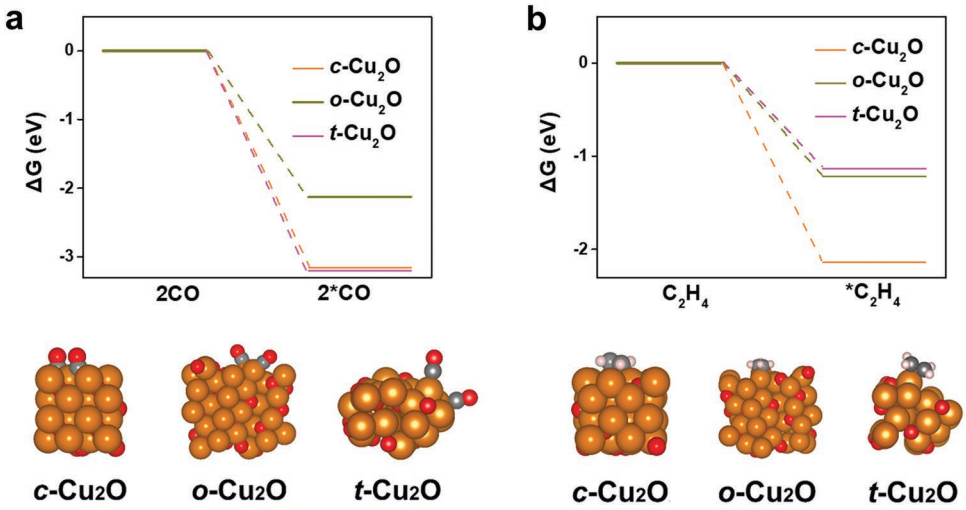

Figure 4. Adsorption energies of a) CO and b) C_2H_4 on the {100} surfaces, {111} surfaces and the interface of {100} and {111} surfaces of Cu_2O. The corresponding adsorption configurations are also shown.

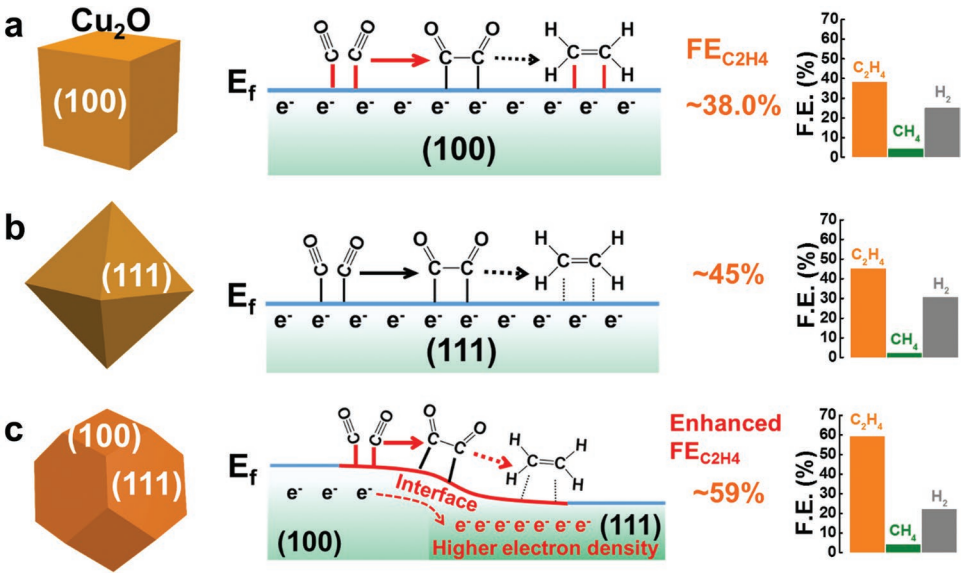

Figure 5. Formation of C_2H_4 on the a) {100} facets of c-Cu_2O NPs, b) {111} facets of o-Cu_2O NPs, and c) {100} and {111} facets of t-Cu_2O NPs.

23.1 mA cm^{-2}, respectively, for the CO_2RR at –1.1 V in 0.5 M $KHCO_3$. These are better than those of the o-Cu_2O NPs with {111} facets (45%, 16.4 mA cm^{-2}) and c-Cu_2O NPs with {100} facets (38%, 10.6 mA cm^{-2}). Our study suggests that the electrocatalytic activity of Cu_2O NPs is an intrinsic property of these oxides rather than the metallic Cu NPs produced on their surfaces during the CO_2RR. The enhanced performance of t-Cu_2O NPs can be attributed to the synergistic effect of {100} and {111} facets, which can not only facilitate the C–C coupling and C_2H_4 desorption, but also be able to promote the multielectron involved kinetics for ethylene production. Our work may provide a new route for enhancing the selectivity of the electrocatalytic CO_2 reduction by crystal facet engineering.

Experimental Section

Preparation of the c-Cu_2O, o-Cu_2O, and t-Cu_2O Particles: Cu_2O particles were synthesized by wet chemical reduction method according to previous reports.[1,2] In a typical synthesis, polyvinylpyrrolidone (PVP, MW 24 000) (0 g for c-Cu_2O, 4 g for t-Cu_2O, and 6 g for o-Cu_2O) was added into 100 mL $CuCl_2 \cdot 2H_2O$ aqueous solution. Then, 10.0 mL NaOH aqueous solution (2.0 M) was added dropwise into the above solution. After stirring for 30 min, 10.0 mL ascorbic acid solution (0.60 M) was added dropwise into the dark brown solution. The mixture was aged for 3 h and the solution gradually transferred into turbid red. All of the procedure was carried out under constant stirring and heated in a water bath at 55 °C. The resulting precipitate was collected by centrifugation and decanting, followed by washing with distilled water 3 times and absolute ethanol 3 times and finally dried under vacuum at 60 °C for 6 h.

Preparation of the Electrodes: Typically, an ink of Cu_2O/C particles was prepared by adding 2 mg catalyst (c-Cu_2O, o-Cu_2O, or t-Cu_2O particles) and 8 mg Carbon Black into the ink-base of 800 µL of isopropanol, 100 µL of H_2O, and 100 µL of 5% nafion solution and then ultrasonicating the solution for 3 h. We deposited 10 µL of the sample inks on the GCE (diameter, 5 mm) to form the sample electrodes.

Electrochemical Experiments: The linear sweeping voltammetry (LSV) measurements were carried out with an Ag/AgCl reference electrode (with saturated KCl as the filling solution), a platinum electrode as the counter electrode and the as-prepared samples as the working electrode. The product analysis was carried out in a two-compartment electrochemical cell with an anion exchange membrane separating the working and counter electrodes. The potentiostatic measurements were performed using a three-electrode system to determine the value of the consumed coulomb, and the amounts of the gases produced were measured by the GC and GCMS instruments. The electrolyte was potassium bicarbonate saturated with CO_2 by bubbling high-purity CO_2 gas, before each experiment, at a flow rate of 50 mL min^{-1} for 1 h to remove all oxygen from the electrolyte. The working electrode was tested 20 times before the plot is recorded at a scan rate of 50 mV s^{-1}. All potentials were transformed to the reversible hydrogen electrode reference by using the calibrated relationship, $E_{RHE} = E_{Ag/AgCl} + 0.657$ V.

Characterization: Crystal structures of the as-obtained products were characterized by XRD measurements with a Bruker AXS D8 diffractometer using Cu Kα radiation. Fourier transform infrared (FTIR) spectra were obtained on a Bruker ALPHA-T spectrometer using KBr pellets. Raman spectra were recorded on a microscopic confocal Raman spectrometer (Horiba JobinYvon, LabRAM HR) with an excitation of 613 nm laser light. Morphologies and microstructures of the products were characterized by scanning electron microscopy (Hitachi S-4800) equipped with an Energy Dispersive Spectrometer (EDS) and transmission electron microscopy using a Philips Tecnai 20U-Twin microscope at an acceleration voltage of 200 kV. (JEOL JEM-2100F). X-ray photoelectron spectroscopy (XPS) measurement was performed using a Thermo Fisher Scientific Escalab 250 spectrometer with monochromatized Al Kα excitation, and C1s (284.6 eV) was used to calibrate the peak positions of various elements. All electrochemical experiments were carried out using the electrochemical workstation CHI660E. The gas products from the compartment were examined with a gas chromatograph equipped with a TDX-01 column with a flame ionization detector (FID) and a H_2-detection GC (ShiweipxGC-7806) with a thermal conductivity detector (TCD). Gas chromatograph-mass spectrometer (GCMS) was used to determine the concentration of liquid products with a Max capillary column.

The faradaic efficiency (FE) was calculated by the following equation

$$FE_{C_2H_4} = \frac{\alpha nF}{Q} = \frac{2nF}{It} \quad (1)$$

Where α is the number of the electrons transferred for CO, F is the Faraday constant, Q is the charge, I is the current, t is the running time, and n is the total amount of CO (in moles).

Supporting Information

Supporting Information is available from the Wiley Online Library or from the author.

Acknowledgements

This work is financially supported by the National Natural Science Foundation of China (21972078 and 21333006), and the Shandong Provincial Natural Science Foundation (ZR2019MEM004). Z.Y.W. acknowledges the support from Shandong University multidisciplinary research and innovation team of young scholars (2020QNQT11), Qilu Young Scholar Program of Shandong University, Young Scholars Program of Shandong University (2015WLJH35) and the Fundamental Research Funds of Shandong University (2018JC039). B.B.H acknowledges the support from the Taishan Scholar Foundation of Shandong Province.

Conflict of Interest

The authors declare no conflict of interest.

Keywords

crystal facets engineering, cuprous oxide, electrocatalytic CO_2 reduction, ethylene, selectivity

Received: October 9, 2019
Revised: January 15, 2020
Published online: January 30, 2020

[1] B. Obama, *Science* **2017**, *355*, 126.
[2] M. Mikkelsen, M. Jørgensen, F. C. Krebs, *Energy Environ. Sci.* **2010**, *3*, 43.
[3] H. Q Yang, Z. H. Xu, M. H. Fan, R. Gupta, R. B. Slimane, A. E. Bland, I. Wright, *J. Environ. Sci.* **2008**, *20*, 14.
[4] J. Qiao, Y. Liu, F. Hong, J. Zhang, *Chem. Soc. Rev.* **2014**, *43*, 631.
[5] L. Zhang, Z. J. Zhao, J. Gong, *Angew. Chem., Int. Ed.* **2017**, *56*, 11326.
[6] S. Chu, Y. Cui, N. Liu, *Nat. Mater.* **2017**, *16*, 16.
[7] C. Liu, B. C. Colon. M. Ziesack, P. A. Silver, D. G. Nocera, *Science* **2016**, *352*, 1210.
[8] S. Gao, Y. Lin, X. Jiao, Y. Sun, Q. Luo, W. Zhang, D. Li, J. Yang, Y. Xie, *Nature* **2016**, *529*, 68.
[9] S. Liu, H. Tao, L. Zeng, Q. Liu, Z. Xu, Q. Liu, J. L. Luo, *J. Am. Chem. Soc.* **2017**, *139*, 2160.
[10] Y. Gao, F. Li, P. Zhou, Z. Wang, Z. Zheng, P. Wang, Y. Liu, Y. Dai, M. Whangbo, B. Huang, *J. Mater. Chem. A* **2019**,*7*, 16685.
[11] Q. Lu, J. Rosen, Y. Zhou, G. S. Hutchings, Y. C. Kimmel, J. G. Chen, F. Jiao, *Nat. Commun.* **2014**, *5*, 3242.
[12] B. A. Rosen, A. Salehi-Khojin, M. R. Thorson, W. Zhu, D. T. Whipple, P J. A. Kenis, R. I. Masel, *Science* **2011**, *334*, 643.
[13] M. Liu, Y. Pang, B. Zhang, P. De Luna, O. Voznyy, J. Xu, X. Zheng, C. T. Dinh, F. Fan, C. Cao, F. P. de Arquer, T. S. Safaei, A. Mepham, A. Klinkova, E. Kumacheva, T. Filleter, D. Sinton, S. O. Kelley, E. H. Sargent, *Nature* **2016**, *537*, 382.
[14] Q. Gong, P. Ding, M. Xu, X. Zhu, M. Wang, J. Deng, Q. Ma, N. Han, Y. Zhu, J. Lu, Z. Feng, Y. Li, W. Zhou, Y. Li, *Nat. Commun.* **2019**, *10*, 2807.
[15] P. D. Luna, C. Hahn, D. Higgins, S. A. Jaffer, T. F. Jaramillo, E. H. Sargent, *Science* **2019**, *364*, eaav3506.
[16] Y. Hori, *Electrochemical CO_2 Reduction on Metal Electrodes*, Modern Aspects of Electrochemistry, Vol. *42* (Eds: C. G. Vayenas, R. E. White, M. E. Gamboa-Aldeco), Springer, New York, NY **2008**.
[17] K. Ogura, H. Yano, F. Shirai, *J. Electrochem. Soc.* **2003**, *150*, D163.
[18] A. A. Peterson, F. Abild-Pedersen, F. Studt, J. Rossmeisl, J. K. Nørskov, *Energy Environ. Sci.* **2010**, *3*, 1311.
[19] K. P. Kuhl, E. R. Cave, D. N. Abram, T. F. Jaramillo, *Energy Environ. Sci.* **2012**, *5*, 7050.
[20] J. Hussain, H. Jónsson, E. Skúlason, *ACS Catal.* **2018**, *8*, 5240.
[21] J. Wang, F. Zhang, X. Kang, S. Chen, *Curr. Opin. Electrochem.* **2019**, *13*, 40.
[22] O. A. Baturina, Q. Lu, M. A. Padilla, L. Xin, W. Li, A. Serov, K. Artyushkova, P. Atanassov, F. Xu, A. Epshteyn, T. Brintlinger, M. Schuette, G. E. Collins, *ACS Catal.* **2014**, *4*, 3682.
[23] Y. X. Duan, F. L. Meng, K. H. Liu, S. S. Yi, S. J. Li, J. M. Yan, Q. Jiang, *Adv. Mater.* **2018**, *30*, 1706194.
[24] Y. Wang, Z. Chen, P. Han, Y. Du, Z. Gu, X. Xu, G. Zheng, *ACS Catal.* **2018**, *8*, 7113.
[25] K. J. Schouten, Z. Qin, E. Perez Gallent, M. T. Koper, *J. Am. Chem. Soc.* **2012**, *134*, 9864.
[26] Y. Hori, I. Takahashi, O. Koga, N. Hoshi, *J. Phys. Chem. B* **2002**, *106*, 15.
[27] X. Liu, J. Xiao, H. Peng, X. Hong, K. Chan, J. K. Norskov, *Nat. Commun.* **2017**, *8*, 15438.
[28] A. Verdaguer-Casadevall, C. W. Li, T. P. Johansson, S. B. Scott, J. T. McKeown, M. Kumar, I. E. Stephens, M. W. Kanan, I. Chorkendorff, *J. Am. Chem. Soc.* **2015**, *137*, 9808.
[29] C. W. Li, J. Ciston, M. W. Kanan, *Nature* **2014**, *508*, 504.
[30] D. Gao, I. Zegkinoglou, N. J. Divins, F. Scholten, I. Sinev, P. Grosse, B. Roldan Cuenya, *ACS Nano* **2017**, *11*, 4825.
[31] H. Mistry, A. S. Varela, C. S. Bonifacio, I. Zegkinoglou, I. Sinev, Y. W. Choi, K. Kisslinger, E. A. Stach, J. C. Yang, P. Strasser, B. R. Cuenya, *Nat. Commun.* **2016**, *7*, 12123.
[32] P. D. Luna, R. Quintero-Bermudez, C. Dinh, M. B. Ross, O. S. Bushuyev, P. Todorović, T. Regier, S. O. Kelley, P. Yang, E. H. Sargent, *Nat. Catal.* **2018**, *1*, 103.
[33] C. Reller, R. Krause, E. Volkova, B. Schmid, S. Neubauer, A. Rucki, M. Schuster, G. Schmid, *Adv. Energy Mater.* **2017**, *7*, 1602114.
[34] Y. Lum, J. W. Ager, *Angew. Chem., Int. Ed.* **2018**, *57*, 551.
[35] Z. Q. Liang, T. T. Zhuang, A. Seifitokaldani, J. Li, C. W. Huang, C. S. Tan, Y. Li, P. De Luna, C. T. Dinh, Y. Hu, Q. Xiao, P. L. Hsieh, Y. Wang, F. Li, R. Quintero-Bermudez, Y. Zhou, P. Chen, Y. Pang, S. C. Lo, L. J. Chen, H. Tan, Z. Xu, S. Zhao, D. Sinton, E. H. Sargent, *Nat. Commun.* **2018**, *9*, 3828.
[36] M. Favaro, H. Xiao, T. Cheng, W. A. Goddard III, J. Yanoa, E. J. Crumlin, *Proc. Natl. Acad. Sci. USA* **2017**, *114*, 6706.
[37] H. Xiao, W. A. Goddard III, T. Cheng, Y. Liu, *Proc. Natl. Acad. Sci. USA* **2017**, *114*, E7045.
[38] H. Jung, S. Y. Lee, C. W. Lee, M. K. Cho, D. H. Won, C. Kim, H. S. Oh, B. K. Min, Y. J. Hwang, *J. Am. Chem. Soc.* **2019**, *141*, 4624.
[39] C. W. Li, M. W. Kanan, *J. Am. Chem. Soc.* **2012**, *134*, 7231.
[40] A. Eilert, F. Cavalca, F. S. Roberts, J. Osterwalder, C. Liu, M. Favaro, E. J. Crumlin, H. Ogasawara, D. Friebel, L. G. M. Pettersson, A. Nilsson, *J. Phys. Chem. Lett.* **2017**, *8*, 285.
[41] Y. Hori, I. Takahashi, O. Koga, N. Hoshi, *J. Mol. Catal. A: Chem.* **2003**, *199*, 39.
[42] W. Huang, *Acc. Chem. Res.* **2016**, *49*, 520.
[43] K. Jiang, R. B. Sandberg, A. J. Akey, X. Liu, D. C. Bell, J. K. Nørskov, K. Chan, H. Wang, *Nat. Catal.* **2018**, *1*, 111.
[44] X. Qin, P. B. Balbuena, M. Shao, *J. Phys. Chem. C* **2019**, *123*, 14449.
[45] Z. Zheng, B. Huang, Z. Wang, M. Guo, X. Qin, X. Zhang, P. Wang, Y. Dai, *J. Phys. Chem. C* **2009**, *113*, 14448.

[46] Z. Wang, G. Yang, Z. Zhang, M. Jin, Y. Yin, *ACS Nano* **2016**, *10*, 4559.
[47] S. Lee, D. Kim, J. Lee, *Angew. Chem., Int. Ed.* **2015**, *54*, 14701.
[48] D. Ren, Y. Deng, A. D. Handoko, C. S. Chen, S. Malkhandi, B. S. Yeo, *ACS Catal.* **2015**, *5*, 2814.
[49] D.-F. Zhang, H. Zhang, L. Guo, K. Zheng, X.-D. Han, Z. Zhang, *J. Mater. Chem.* **2009**, *19*, 5220.
[50] J. Lin, W. Hao, Y. Shang, X. Wang, D. Qiu, G. Ma, C. Chen, S. Li, L. Guo, *Small* **2018**, *14*, 1703274.
[51] Y. Sui, W. Fu, Y. Zeng, H. Yang, Y. Zhang, H. Chen, Y. Li, M. Li, G. Zou, *Angew. Chem., Int. Ed.* **2010**, *49*, 4282.
[52] P. Zhou, D. Xing, Y. Liu, Z. Wang, P. Wang, Z. Zheng, X. Qin, X. Zhang, Y. Dai, B. Huang, *J. Mater. Chem. A* **2019**, *7*, 5513.
[53] S. Back, M. S. Yeom, Y. Jung, *ACS Catal.* **2015**, *5*, 5089.
[54] H. L. Skriver, N. M. Rosengaard, *Phys. Rev. B* **1992**, *46*, 7157.
[55] N. Shehzad, M. Tahir, K. Johari, T. Murugesan, M. Hussain, *J. CO2 Util.* **2018**, *26*, 98.
[56] Z. Xiong, Z. Lei, C.-C. Kuang, X. Chen, B. Gong, Y. Zhao, J. Zhang, C. Zheng, J. C. S. Wu, *Appl. Catal., B* **2017**, *202*, 695.
[57] S. Xie, Y. Wang, Q. Zhang, W. Deng, Y. Wang, *ACS Catal.* **2014**, *4*, 3644.